Ecological Monographs, 87(1), 2017, pp. 21–33

Physical calculations of resistance to water loss improve predictions of species range models

Eric A. Riddell,[1] Evan K. Apanovitch, Jonathan P. Odom, and Michael W. Sears

Department of Biological Sciences, Clemson University, 132 Long Hall, Clemson, South Carolina 29634 USA

Abstract. Species ranges are constrained by the physiological tolerances of organisms to climatic conditions. By incorporating physiological constraints, species distribution models can identify how biotic and abiotic factors constrain a species' geographic range. Rates of water loss influence species distributions, but characterizing water loss for an individual requires complex calculations. Skin resistance to water loss (r_i) is considered to be the most informative metric of water loss rates because it controls for experimental biases. However, calculating r_i requires biophysical equations to solve for the resistance of the air that surrounds an organism, termed the boundary layer resistance (r_b). Here, we compared theoretical and empirical methods for measuring skin resistance to water loss of a *Plethodon* salamander collected from nature. For the empirical methods, we measured r_b of agar replicas at five body sizes, two temperatures, three vapor pressure deficits, and six flow rates using a flow-through system. We also calculated r_b using biophysical equations under the same experimental conditions. We then determined the ecological implications of incorporating skin and boundary layer resistance into a species range model that estimated potential activity time and energy balance throughout the geographic range of the study species. We found that empirical methods for calculating r_b resulted in negative values of r_i, whereas biophysical calculations produced meaningful values of r_i. The species range model determined that ignoring realistic boundary layer and skin resistances reduced average estimates of energy balance by as much as 64% and potential activity time by 88% throughout the spatial extent of the model. We conclude that the use of agar replicas is an inadequate technique to characterize skin resistance to water loss, and incorporating boundary layer and skin resistances to water loss improves estimates of activity and energetics for mechanistic species distribution models. More importantly, our study suggests that incorporating the physical processes underlying rates of water loss could improve estimates of habitat suitability for many animals.

Key words: biophysics; energy budget; physiological ecology; salamander; skin resistance; species distribution models; water loss.

Introduction

A fundamental problem in ecology is to identify the factors that determine the uneven distribution of organisms through space and time (Scheiner 2010). Climate influences a species' distributions by threatening an organism's physiological capacity to survive (Grinnell 1917). By incorporating physiology, species distribution models (SDMs) can identify the interactions between an organism's biology and local climate that limit geographic distributions (Kearney and Porter 2004, 2009, Crozier and Dwyer 2006, Buckley et al. 2010). These models take advantage of the relationships between physiological traits and temperature to identify regions in which organisms remain in positive energy balance. Rates of water loss are a major determinant of energy balance because they influence how long an individual can forage (Kearney and Porter 2004, Gifford and Kozak 2012). By knowing energy intake and expenditure, these models determine whether individuals can forage long enough to offset energy expenditure. Geographic regions with positive energy or water balance identify potentially suitable habitat because individuals have energy available for reproduction. However, SDMs grounded in physiology rely upon accurate characterization of the traits that link organisms to their environment. Water loss rates are difficult to measure because they require complex calculations or physical models of the study organism (Spotila and Berman 1976, Wygoda 1984, Tracy et al. 2010*a*). Many studies have advanced the calculations required for studying water loss (Tracy 1975, 1976, 1982), yet calculations of important physical processes involved in water loss are still lacking.

Not all methods for characterizing water loss traits are equal because most are influenced by body size, humidity, wind speed, and temperature (Feder and Burggren 1992). Therefore, these factors preclude comparisons of some water loss traits (e.g., cutaneous water loss rates) among experiments. Skin (or integumentary) resistance to water loss (r_i) is considered to be the most biologically informative metric for characterizing water loss physiology because it integrates the biological processes underlying water loss rates (Gates 1980, Feder and Burggren 1992,

Manuscript received 28 September 2016; accepted 29 September 2016. Corresponding Editor: Aimée T. Classen.
[1]E-mail: eriddel@clemson.edu

Tracy et al. 2007, Hillman et al. 2009). Therefore, r_i is generally considered to be the most informative metric of water loss for comparisons across taxa and experiments (Lillywhite 2006). However, calculating r_i is challenging due to the dynamics of the air surrounding the organism. Total resistance (r) is the sum of r_i and the resistance of the boundary layer (r_b) of air surrounding the organism (Gates 1980, Feder and Burggren 1992). In terrestrial environments, the boundary layer is the layer of air in which the organism (or any object) exchanges heat and mass with its surrounding environment. The boundary layer adds to the resistance of water loss by changing the physical conditions of the microclimate around the organism. Thus far, SDMs grounded in biological mechanisms have not considered the ecological significance of the boundary layer despite its potential to reduce water loss for many taxa.

Physical surrogates, such as agar replicas of the model organism, are frequently used to calculate r_b as well as to understand ecological processes, such as species distributions (Young et al. 2005, 2006), physiological adaptations (Amey and Grigg 1995, Christian and Parry 1997), microhabitat selection (Seebacher and Alford 2002), and physiological responses to temperature (Buttemer 1990). Spotila and Berman (1976) pioneered the use of agar replicas as physical surrogates due to its apparent negligible resistance to water loss. However, agar models clearly exhibit a resistance to water loss, even when compared to other physical surrogates (Tracy et al. 2007). Despite agar's poor performance relative to other physical surrogates, we know very little about the consequences of using physical surrogates in ecological studies.

Estimating the water flux using biophysics requires detailed equations on interacting physical factors, such as temperature and humidity (Tracy 1976, Gates 1980). For instance, air temperature limits the amount of water vapor that the air can hold. As air temperature warms, the capacity of the air to hold vapor increases exponentially. Once the amount of vapor reaches this capacity, termed the saturation water vapor pressure (e_s), vapor in the air must condense into liquid (Stull 2000). This concept is critical to understanding the physical processes that drive evaporative water loss because the difference between e_s and the actual amount of vapor in the air drives evaporation rates. This difference is termed the vapor pressure deficit (VPD; Anderson 1936). Simply based on physics, warm air is more likely to have greater drying power than cool air. These dynamics are known to influence animal ecology because animals limit foraging activity under high VPDs (Riddell and Sears 2015) and breeding activities to cool times of day when VPDs are low (Bellis 1962). Therefore, physical interactions have ecological implications for activity and energetics of animals.

To evaluate the effectiveness of physical surrogates, we compared theoretical calculations to empirical methods for estimating r_i of a *Plethodon* salamander. We measured boundary layer resistance of five body sizes of agar replicas under two temperatures, three vapor pressure deficits, and six flow rates (convective environments) using a flow system capable of precisely controlling temperature and vapor pressure. For theoretical methods, we used dimensionless analysis to calculate the boundary layer resistance under free and forced convection. Then we calculated skin resistance of live salamanders using empirical and theoretical methods, and we found that using agar resulted in negative values of r_i for nearly one-half of the individuals. Negative skin resistances are nonsensical because they suggest salamanders have higher water loss rates than free water. Finally, we demonstrate the ecological significance of accurate estimates of resistances using a physiologically structured species distribution model. Our analyses determined that calculations of the boundary layer and accurate estimates of skin resistances have major implications for estimating activity time and energy balance of animals, which are major determinants of mechanistic species range models.

Materials and Methods

Comparisons of empirical and theoretical values

We calculated the skin resistance to water loss (r_i) from rates of water loss for salamanders (*P. metcalfi*) collected from the field during a previous experiment on salamander water loss physiology (Riddell and Sears 2015). The design of the flow-through system for the agar replicas was identical for determining water loss rates of salamanders except we only used one flow rate (180 mL/min) on the salamanders. A detailed description of the flow-through system, experimental design, and collection can be found in Riddell and Sears (2015). We then used estimates of r_b from theoretical and empirical methods to determine the consequence of using either method.

Construction of agar replicas

We estimated empirical values of boundary layer resistance by conducting experiments on agar replicas of *Plethodon jordani* specimens provided by the Campbell Museum of Natural History at Clemson University. We made agar replicas of differently sized salamanders by developing a cast using alginate (Spotila and Berman 1976). After mixing the alginate, we allowed the alginate to dry for 3–5 min and placed the specimen into the alginate. We then poured a second layer of alginate on top of the specimen. After hardening, the specimen was removed by carefully separating the primary and secondary layers of alginate. We used a 3% agar solution during our experiments because of its previously reported negligible resistance to water loss (Spotila and Berman 1976). We injected the agar solution into the mold at the ends of the cast through small holes made in the secondary layer of alginate. We carefully trimmed each agar model to ensure a similar size and surface features among replicates of the agar models. Due to the fragility of the

legs, we trimmed the legs from each agar to ensure similar surface features. Removal of the legs is likely inconsequential to influencing the estimates of the boundary layer because the posture of agar models was similar to the focal species during experiments. The relationship between snout–vent length and mass between *P. jordani* specimens and *P. metcalfi* collected from nature were indistinguishable in our study (Appendix S1: Fig. S1).

Flow-through system and experimental design

We used a flow-through system capable of precisely controlling water vapor pressure, flow rate, and temperature to empirically measure r_b. In the system, we started with a sub-sampler (SS-4; Sable Systems International (SSI), 3840 N. Commerce Street, North Las Vegas, NV 89032 USA) to push air through a dewpoint generator (DG-4; Sable Systems) capable of precisely controlling water vapor pressure. With the dewpoint generator, we adjusted the relative humidity to measure water loss at specific vapor pressure deficits. We calculated VPDs using

$$\mathrm{VPD} = e_s - e_a \quad (1)$$

where e_s is the saturation vapor pressure (kPa) at a given temperature and e_a is the vapor pressure of ambient air (kPa). To calculate e_s, we used the Clausius-Clapeyron equation (Stull 2000)

$$e_s = e_0 \cdot \exp\left[\frac{L}{R_v}\left(\frac{1}{T_0} - \frac{1}{T}\right)\right] \quad (2)$$

where $e_0 = 0.611$ kPa and $T_0 = 273$ K are constant parameters, and $R_v = 461.5\ \mathrm{J{\cdot}K^{-1}{\cdot}kg^{-1}}$ and $L = 2.5 \times 10^6$ J/kg are the gas constant for water vapor and the latent heat of vaporization, respectively.

We then used a manifold (MF-8; SSI) to split the airstream and control flow rates among eight chambers. Each airstream then passed through an acrylic cylindrical chamber (16 × 3.5 cm; volume ~153 mL) containing the agar model. The agar models were supported on top of hardwire mesh to ensure that the entire surface area of the agar model contacted the airstream, similar to previous methods on salamanders (Riddell and Sears 2015). We then sampled each chamber every eight minutes using a multiplexer (MUX-8; SSI). Each airstream then passed through a water vapor analyzer (RH-300; SSI) to measure the change in water vapor pressure attributed by the agar replica. The RH-300 was spanned with the DG-4 at the beginning of the experiment and zeroed using columns of Drierite (W.A. Hammond Drierite Co. Ltd., P.O. Box 460 Xenia, OH 45385, USA) each day before the experiment. Finally, we measured the flow rate of the air using the flow meter within the SS-4 after the air had been scrubbed of water vapor.

We conducted two separate experiments to measure (1) the effect of flow rate and (2) the effect of temperature and VPD on boundary layer resistance. Each experiment measured r_b across the spectrum of body sizes. We determined the boundary layer resistance for five different body sizes of agar replicas (0.50, 1.02, 1.28, 2.51, and 2.82 g), three VPDs (0.20, 0.35, and 0.50 kPa), two temperatures (12°C and 18°C), and six flow rates (50, 100, 200, 300, 400, and 500 mL/min). We randomized the order of the experiments with respect to body size, temperature, water vapor pressure, and flow rate to minimize the possibility of systematic errors in the measurements. We validated the VPD treatments by placing hygrochron iButtons (Maxim Integrated, 160 Rio Robles, San Jose, CA 95134 USA) at the incurrent and excurrent portions of the chamber. We then compared the vapor pressures measured at these locations to make sure that we created the desired vapor gradient (Appendix S1: Fig. S2). Air temperatures inside the chamber were monitored using the thermocouple on the DG-4 (Sable Systems) and validated with a hygrochron (Maxim Integrated) inside the chamber.

Empirical calculations of skin resistance to water loss

Calculating the resistance of the skin to water loss relies upon specific values from the agar model and the environment. We calculated the water vapor density (ρ_v; g/mL) evaporating from the agar model using the change in water vapor pressure (e; kPa) between the incurrent and excurrent water vapor pressure. The difference in e corresponded to the amount of water vapor evaporating from the surface of the agar replica. Water vapor density was calculated as

$$\rho_v = \frac{e}{(T \times R_v)} \quad (3)$$

where T is temperature in Kelvin (K) and R_v is the gas constant for water vapor ($461.5\ \mathrm{J{\cdot}K^{-1}{\cdot}kg^{-1}}$). To calculate total mass lost from evaporative water loss (EWL; g/s), we used the following equation:

$$\mathrm{EWL} = \rho_v \times \mathrm{FR} \times \frac{1}{60} \quad (4)$$

where FR is the flow rate of the air stream (mL/min), followed by a conversion factor for mg/min (Bernstein et al. 1977). To calculate CWL ($\mathrm{g{\cdot}s^{-1}{\cdot}cm^{-2}}$), we divided the rate of water loss by the estimated surface area of each salamander. The surface area ($\mathrm{cm^2}$) was estimated by an empirically derived formula for the family Plethodontidae, where surface area = 8.42 × mass $(\mathrm{g})^{0.694}$ (Whitford and Hutchison 1967). The empirical estimates of boundary layer were calculated from

$$r = r_i + r_b = \frac{\rho}{\mathrm{CWL}} \quad (5)$$

where ρ is the vapor density gradient ($\mathrm{g/cm^3}$) and CWL is the cutaneous water loss rate ($\mathrm{g{\cdot}cm^{-2}{\cdot}s^{-1}}$; Feder and Burggren 1992). To calculate r_b of the agar replicas, empirical methods assume that agar lacks a skin resistance to water loss. Consequently, r_b and the total resistance (r) are calculated using the same formulas under the assumption that agar does not have a skin resistance, and therefore, $r = r_b$.

Theoretical methods for calculating the boundary layer

The physical properties of the environment that surround an organism determine the rates of energy and mass flux. For terrestrial organisms, the viscosity of the air, temperature, water vapor pressure, wind speed, and body size of the organism determine the exchanges of heat and mass with the environment. As air passes over the organism, the viscosity of the fluid produces a drag force, slowing the rate of the fluid over the organism, described as the boundary layer (Gates 1980). The rate at which the air passes over the animal also determines whether forced or free convection primarily influences boundary layer dynamics. Therefore, we present separate calculations for both types of convection.

Calculations of the boundary layer resistance require equations using a series of dimensionless values. To make these calculations feasible, the dimensions of the organism are assumed to be that of a cylinder, an adequate approximation for many small animals (Gates 1980). Here, we present two series of equations representing the boundary layer resistance under forced and free convection. Symbol definitions for all equations can be found in Table 1. Each of these equations depends upon the kinematic viscosity of the air (v; m^2/s), which is calculated as

$$v = \frac{\mu}{\rho} \tag{6}$$

where μ is the dynamic viscosity of air ($kg \cdot m^{-1} \cdot s^{-1}$) and ρ is the density of air (kg/m^3; Tracy et al. 2010*b*). The dynamic viscosity of air is calculated as

$$\mu = \mu_0 \left[\frac{T_0 + C}{T + C} \left(\frac{T}{T_0} \right)^{1.5} \right] \tag{7}$$

Table 1. List of symbols and definitions used in theoretical methods.

Symbol	Definition
r_b	boundary layer resistance
ρ	water vapor density gradient
C_ρ	specific heat at constant pressure
h_c	convection coefficient
Gr	Grashof number
k	thermal conductivity of air
D	characteristic dimension
g	acceleration by gravity
β	volumetric thermal expansion
ΔT	difference in temperature between organism and environment
v^2	kinematic viscosity
T_0	temperature of surface losing heat to environment
e_0	partial pressure of water vapor on surface losing water to environment
p	atmospheric pressure
e	water vapor pressure
T	temperature
r_i	skin resistance to water loss
EWL	evaporative water loss
CWL	cutaneous water loss
μ	viscosity coefficient
SA	surface area

where T is the temperature (K), μ_0 is the constant 1.8325×10^{-5}, T_0 is the constant 296.16, and C is a constant at 120 (Tracy et al. 2010*b*). The pressure of air is calculated as

$$p = 101{,}325[1 - (2.2569 \times 10^{-5} \times Z]^{5.2553} \tag{8}$$

where Z is the altitude (m) between −1000 and 20 000 m (Tracy et al. 2010*b*).

Free convection

Dimensionless analysis must be used to determine the boundary layer resistance (r_b) under free convection conditions. During free convection, the organism changes the composition of the air through the transfer of heat or evaporation, forcing the movement of air away from the surface of the organism. The Grashof number describes the relative strengths of the buoyant forces to the viscous force of the air surrounding an object (Gates 1980). The Grashof number is calculated as

$$\mathrm{Gr} = \frac{g \times \beta \times \Delta T \times D^3}{v^2} \tag{9}$$

where g is the acceleration by gravity (9.80 m/s^2), β is the coefficient of volumetric expansion (3.67×10^{-3} $°C^{-1}$), D is the characteristic dimension, and v is the kinematic viscosity (Gates 1980). For a cylinder, the characteristic dimension is the cross-sectional radius (Gates 1980). To determine the radius of a salamander, we anaesthetized salamanders using buffered 0.01% MS-222 solution. Salamanders were then fully submerged in a graduated cylinder to measure the volume of water displaced by the salamander. We then calculated the radius from the volume of the salamander assuming the dimensions of a cylinder. Calculating the Grashof value requires information on the vapor gradient and temperatures of the surface of the organism and air for an organism in steady state heat balance (Monteith and Unsworth 2013). The ΔT can be estimated using

$$\Delta T = T_0(1 + 0.38 \times e_0/p) - T(1 + 0.38 \times e/p) \tag{10}$$

where T_0 is the temperature (K) of the surface, e_0 is the water vapor pressure directly above the surface, and p is the atmosphere pressure (Monteith and Unsworth 2013). From this point, the free convective heat-transfer coefficient can be calculated using

$$h_c = \frac{0.48 \times \mathrm{Gr}^{0.25} \times k}{D} \tag{11}$$

where Gr is the Grashof number, k is the thermal conductivity of the fluid ($W \cdot m^{-1} \cdot K^{-1}$) and D is the characteristic dimension (m). As a note, $0.48 \times \mathrm{Gr}^{0.25}$ represents the Nusselt number, another dimensionless value (Gates 1980). The resistance of the boundary layer can then be calculated using

$$r_b = \frac{0.93 \times \rho C_\rho}{h_c} \tag{12}$$

where ρ is the density of the air and C_ρ is the specific heat of air (Tracy et al. 2010*b*).

Forced convection

As the wind speed of the air increases, the boundary layer dynamics primarily become a function of the velocity of the air and the size of the organism. To calculate forced convection, the specific heat of air (C_ρ) must be calculated as

$$C_\rho = \frac{1004.84 + (1846.40 \times r_w)}{1 + r_w} \quad (13)$$

where T is air temperature (°C) and r_w is mixing ratio of water vapor (Tracy et al. 2010*b*). The mixing ratio can be estimated using

$$r_w = \frac{0.6257 \times e}{p - (1.006 \times e)} \quad (14)$$

where e is the vapor pressure (kPa) and p is the atmospheric pressure (kPa) (Tracy et al. 2010*b*). For forced convection, the coefficient of convective-heat transfer can be approximated using

$$h_c = 0.923(V^{0.333} \times D^{-0.666}) \quad (15)$$

where V is the wind speed (m/s) and D is the characteristic dimension (m). The coefficient of convective heat transfer for forced convection can then be used to calculate r_b using Eq. 13. Boundary layer resistances were calculated assuming free convection conditions. We determined that free convection was the dominant process shaping the boundary layer by comparing Grashof and Reynolds values across all body sizes, flow rates, and vapor pressures. Specifically, we used the relationship

$$\mathrm{Gr} > 16 \times \mathrm{Re}^2$$

to determine if free convection is the dominant force shaping the boundary layer (Gates 1980). In this equation, Gr refers to the Grashof number and Re refers to the Reynolds number, which are both dimensionless values. If the inequality is true, then free convection characterizes the dynamics within the boundary layer. For our experimental treatments, the Grashof number ranged from 1.9 to 386.8 and values calculated from the Reynolds number ranged from 0.35 to 4.9. In every case, the Grashof number was greater than the values calculated from the Reynolds number, indicating that free convection should characterize the dynamics of the boundary layer resistance in our experiments.

Species distribution model

We evaluated the ecological importance of resistances to water loss by estimating potential activity time and net energy balance throughout the geographic range of *P. metcalfi* using a biophysical model. In the model, we calculated the amount of time an average adult salamander (3 g) could be active on the forest floor until losing 3.8% of their body mass to water loss, the average threshold at which an adult salamander ceases activity (Feder and Londos 1984). Estimates of activity time and energetics were calculated from scenarios that included salamanders without skin resistance to water loss (i.e., free water, r_s = 1 s/cm) and average skin resistance from our study calculated from first principles (r_s = 5 s/cm). The model also evaluated the contribution of the boundary layer resistance to activity and energetics because current distribution models for salamanders have not considered boundary layer dynamics (Gifford and Kozak 2012). Therefore, the species distribution model was developed to explicitly test the ecological significance of boundary layer resistance and accurate estimates of skin resistance to water loss.

Energy balance of animals are based upon net energy intake while active and energy expenditure. We estimated energy balance based upon previously developed models for energy intake and expenditure that are used in salamander distribution modeling (Gifford and Kozak 2012). Energy expenditure was calculated from standard metabolic rates of oxygen consumption (VO_2; mL O_2/h) that incorporate temperature and mass using

$$\log_{10}\mathrm{MR} = 0.036(T) + 0.57(\log_{10} M) - 1.95 \quad (16)$$

where T is temperature (°C) and M is mass (g) (Gifford and Kozak 2012). We assumed a respiratory quotient of 0.8 (i.e., a mixed diet of fats and carbohydrates) to calculate energetic costs (in joules) from volume of oxygen consumption (de V Weir 1949). Estimates of foraging intake (FI; $\mathrm{cal \cdot g^{-1} \cdot d^{-1}}$) were based upon empirically derived relationships between temperature and energy intake for *Plethodon* salamanders using

$$\mathrm{FI} = 0.015(T^3) - 0.81(T^2) + 12.76(T) - 43.06 \quad (17)$$

where T is temperature (°C; Merchant 1970, Gifford and Kozak 2012). In the model, salamanders rehydrate while active by absorbing water from their ingested food. We assumed salamanders consume insects that consist of 70% water with an average of 2.33 mL H_2O/g dry mass (Bell 1990). With the average insect yielding 22 kJ/g dry mass, we estimated the mass of water absorbed per Joule while the salamander was active (Bell 1990). The biophysical model calculated activity time and energy balance for every second of the night throughout the geographic extent of the model.

Environmental data for the biophysical model were based upon average temperatures and humidities from the microclim data set (Kearney et al. 2014). We estimated activity and energetics using hourly climatic conditions from 2100 to 600 for average conditions in August, the month in which we measured rates of water loss from salamanders in the field. The temperature and humidity estimates were calculated for conditions at 1 cm above the surface of soil in 75% shade cover. To calculate higher resolution temperature data, we corrected the temperature data set from microclim for changes in

elevation using adiabatic lapse rates for dry air. The adiabatic lapse rate describes the change in temperature with altitude assuming there is no heat transfer to or from the air parcel. The corrected temperature values were calculated using

$$T_{\text{final}} = T_{\text{initial}} - (9.8°\text{C/km}) \times \Delta z \quad (18)$$

where Δz is the difference in elevation (Stull 2000). We assumed the vapor content of the air remained constant to calculate the vapor pressure deficits. Our incorporation of the dry (as opposed to wet) adiabatic lapse rate is appropriate because average humidities were never fully saturated. To calculate the difference in elevation, we determined the average elevation that Kearney et al. (2014) used to estimate global temperature values by calculating the average elevation at the same resolution as the microclim data set (10 arc mins or 15 km^2 in the spatial extent of our study). We then subtracted the average elevation from a high-resolution digital elevation map (1/3 arcsecs) to produce a high-resolution raster of the differences in elevation used in Kearney et al. (2014). This digital elevation map of differences was used to estimate temperatures per square kilometer using the adiabatic lapse rate correction. For humidity, we used the relative humidity data from the microclim data set to calculate vapor pressure deficit rasters for each hour using the high resolution temperature rasters. Geographic data were manipulated and visualized using QGIS (Quantum GIS Development Team 2015), and the biophysical models were implemented using custom code for Python (Python Software Foundation 2015).

We included known collection points for *P. metcalfi* to evaluate the estimates of activity and energetics. The coordinates for known collections were downloaded from VertNet, which included 7422 captures from 1931 to present day (data *available online*).[2] Nearly 15% of the captures occurred outside of the geographic range of *P. metcalfi* because, prior to Highton and Peabody (2000), *P. metcalfi* was not recognized as a separate species from the *P. jordani* species complex. Therefore, the captures outside of the geographic range likely represent similar species from the same genus or hybrids between related species. The species range for *P. metcalfi* was downloaded from the IUCN database, and we updated the distribution to include areas indicated to be *P. metcalfi* from allozyme data (Highton and Peabody 2000). We also generated random coordinates throughout the spatial extent of the model to assess the performance of the model at predicting energy budgets across VPDs. These coordinates were used in a logistic regression to determine the relationship between VPD and energy balance.

Statistical methods

We performed all statistical analyses using R (R Core Team 2015). Separate analyses were conducted on the flow rate and VPD experiments. We used nonlinear regression models to meet the assumptions of normality for statistical analyses. Resistance of agar was analyzed with an analysis of covariance (ANCOVA) in which we treated surface area and flow rate as covariates. We also analyzed resistance of agar using an ANCOVA with VPD and temperature as factors and surface area as a covariate. To perform the ANCOVA, we used a type II SS analysis of variance from the car package (Fox and Weisberg 2011) for independent tests of interactions (Langsrud 2003). We then compared empirical and theoretical methods by calculating r_i of salamanders using both methods. We performed linear regression with method (i.e., theoretical, empirical) as a factor and surface area as a covariate. We also calculated effect sizes using

$$\omega^2 = \frac{SS_{\text{treat}} - df_{\text{treat}} \times MS_{\text{err}}}{SS_{\text{tot}} + MS_{\text{err}}} \quad (19)$$

where SS_{treat} is the sum of squares for a given parameter, df_{treat} is the degrees of freedom for that parameter, MS_{err} is the mean square error, and SS_{tot} is the total sum of squares (Olejnik and Algina 2003). For the logistic regression analysis, we report a pseudo-R^2 value (known as the Nagelkerke R^2), which is calculated from the ratio of log-likelihoods using the rms package in R.

Results

Comparison of methods for calculating resistances

We found that using agar produced substantially lower estimates of r_i for salamanders compared to using theoretical methods (Table 2). By using agar, empirical methods resulted in negative skin resistances in nearly half of the individuals, whereas theoretical methods did not produce negative skin resistances (Fig. 1). In addition, r_i varied with body size using theoretical methods, but in contrast, r_i did not vary using empirically based methods. The r_i values from empirical methods are nonsensical from the perspective of physics.

Empirical methods for calculating the boundary layer resistance were quantitatively different from estimates using theoretical methods. We found that flow rate and the boundary layer resistance of agar were negatively associated with one another (Fig. 2A). The analysis underscores the influence of flow rates on water loss

Table 2. Empirical and theoretical methods explained the greatest proportion of variation in estimates of skin resistance to water loss.

Effects	df	SS	*F*	*P*	ω^2
Surface area	1	73.7	8.6	<0.001	0.029
Method	1	612	72	<0.001	0.32
Surface area × method	1	49.7	5.9	0.02	0.017
Residuals	130	1102			

Note: df, degrees of freedom; SS, sum of squares; ω^2, effect size. The threshold for statistical significance $P < 0.05$.

[2] http://vertnet.org

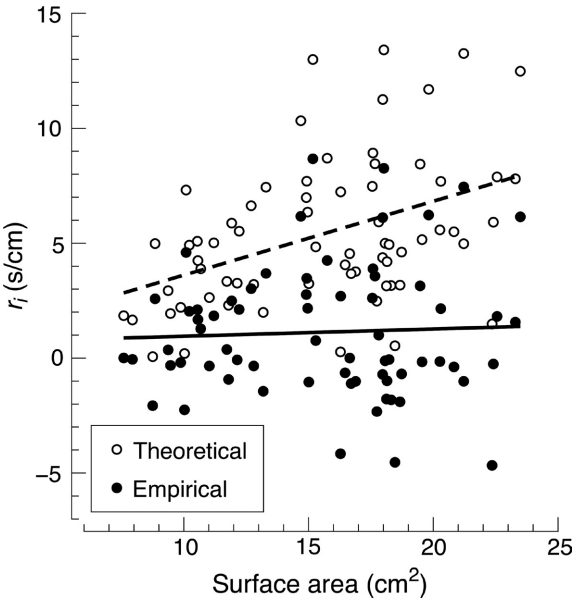

FIG. 1. A comparison of skin resistance (r_i) values calculated from theoretical and empirical methods regressed against surface area of the individual. The figure demonstrates that almost half of the values calculated from empirical methods using agar resulted in negative skin resistance to water loss. The regression also shows that empirical methods result in no relationship between r_i and body size.

dynamics because the flow rate explained the largest portion of the variance in boundary layer resistance (Table 3). However, based upon comparing dimensionless values, the boundary layer at these flow rates should be mostly shaped by free convection (Fig. 2B). Therefore, the variation in the estimated boundary layer from the empirical experiments may be due to additional physical factors (see *Discussion*). Theoretical and empirical values agreed qualitatively by estimating large body sizes to have higher resistances than small body sizes. However, empirical and theoretical methods clearly produce vastly different quantitative estimates of the boundary layer (Fig. 2). The theoretical values of r_b also correspond to expected values of boundary layer resistances for small organisms (Gates 1980, Feder and Burggren 1992).

Our experiments on the effect of vapor pressure deficit on r_b also found quantitative differences between empirical and theoretical methods (Fig. 3). Agar models produced estimates of the boundary layer that were over three times higher than theoretical calculations. However, the relationship between r_b of agar and vapor pressure deficit was qualitatively similar to values from theoretical methods. Specifically, we found that the boundary layer resistance was higher under lower vapor pressure deficits (i.e., moist air). The analysis also shows the surface area of the agar model explained the vast majority of the variation in empirical estimates of r_b (Table 4). Thus, flow rate and body size have a substantial influence on empirical estimates of the boundary layer. Our experiment confirmed that the agar replicas did not saturate the chamber because the vapor concentrations of the incurrent airstreams remained at the desired value upon placing the largest agar model in the chamber (Appendix S1: Fig. S2). These results support our experimental design by validating our control of the environment inside the chamber.

Species distribution model

Incorporating the boundary layer and realistic skin resistances into the species distribution model increased geographic areas where individuals could achieve positive energy balance by 30.4% throughout the geographic

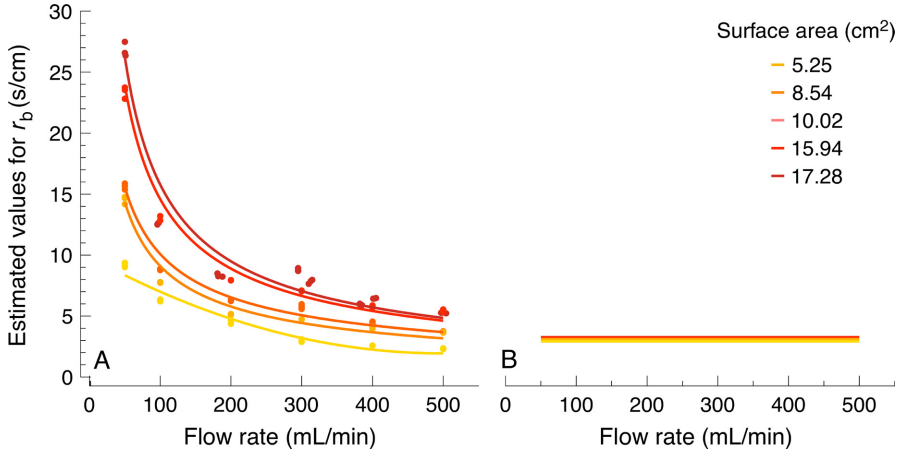

FIG. 2. Estimates of boundary layer resistance (r_b) varying with flow rate using (A) empirical and (B) theoretical methods. Surface areas are shown in different colors, ranging from dark red as the largest to yellow as the smallest. In both cases, large individuals have the largest boundary layer, and high flow rates have the smallest boundary resistance. The two methods differ substantially in their quantitative estimates of the boundary layer resistance. The values of r_b do not vary under theoretical methods because free convection is the dominant force shaping the boundary layer. (Color figure can be viewed at wileyonlinelibrary.com.)

TABLE 3. Experimental flow rate and surface area (cm^2) of agar replicas explain the majority of variation of resistance to water loss.

Effects	df	SS	*F*	*P*	ω^2
Surface area	1	1.96	1149	<0.001	0.31
Log (flow rate)	1	4.22	2476	<0.001	0.66
Surface area × log (flow rate)	1	0.0017	1.021	0.31	<0.01
Residuals	101	0.17			

Note: df, degrees of freedom; SS, sum of squares; ω^2, effect size. The threshold for statistical significance $P < 0.05$.

TABLE 4. Surface area has the highest influence on the boundary layer of agar replicas; temperature does not influence resistance if controlling for VPD.

Effects	df	SS	*F*	*P*	ω^2
Temperature	1	0.0182	0.293	0.59	<0.01
VPD	2	2.26	18.2	<0.001	0.037
Surface area	1	26.0	420	<0.001	0.66
Surface area^2	1	1.74	28.1	<0.001	0.034
Surface area^2 × VPD	2	0.704	5.68	0.004	<0.01
Residuals	126	7.81			

Note: df, degrees of freedom; SS, sum of squares; ω^2, effect size. The threshold for statistical significance $P < 0.05$.

extent of the model. In addition, the estimates of potential activity time increased by 7–10× by including boundary and skin resistances (Fig. 4). Models with and without resistances produced similarly low estimates of energy balance in regions known for low abundances of salamanders (i.e., low elevations and latitudes), but models without resistances underestimated energy balance by an order of magnitude in regions associated with high salamander abundances, such as high elevations (Fig. 4). Also, the results demonstrate that ignoring realistic boundary layer and skin resistances underestimates potential activity time by 88% (Fig. 5). The model also estimated a 64% reduction in net energy balance without realistic resistances (Fig. 5). The incorporation of water absorbed from prey increased activity and energy budgets by 1–8% (depending on area relative to models with realistic resistances to water loss. The greatest increase in activity and energy due to absorbed water from prey occurred at the highest elevations. The results also demonstrate VPD predicted the geographic locations with positive energy balance (Fig. 6; $\beta = -305.8$; SE = 26.9; $P < 0.001$, $R^2 = 0.97$). In addition, of the 7,422 historical captures, 93% occurred in locations estimated to have a positive net energy balance upon including boundary and realistic skin resistances.

DISCUSSION

Our results demonstrate that boundary layer and skin resistances have the potential to be a major determinant of potential activity time and energy balance. By using resistances to water loss from our experimental comparisons, we found that assuming the resistance of free water ($r_i = 1$ s/cm) is likely an inaccurate characterization of water loss, and subsequently, estimates of species range dynamics may be compromised. The historical captures validated our estimates of energy balance with the vast majority of captures occurring in regions estimated to have positive energy balance. The randomly generated coordinates demonstrated that energy balance was tightly associated with VPD (Fig. 6), which is consistent with our knowledge of salamander ecology. Captures from regions with negative energy values may be due to factors that were not considered in the model, such as microhabitat conditions or local changes in food abundance. In addition, our model only considers climatic conditions in August, the time period over which we measured rates of water loss in salamanders. Because August is one of the warmest and driest months of the year, we expect our estimates to be conservative

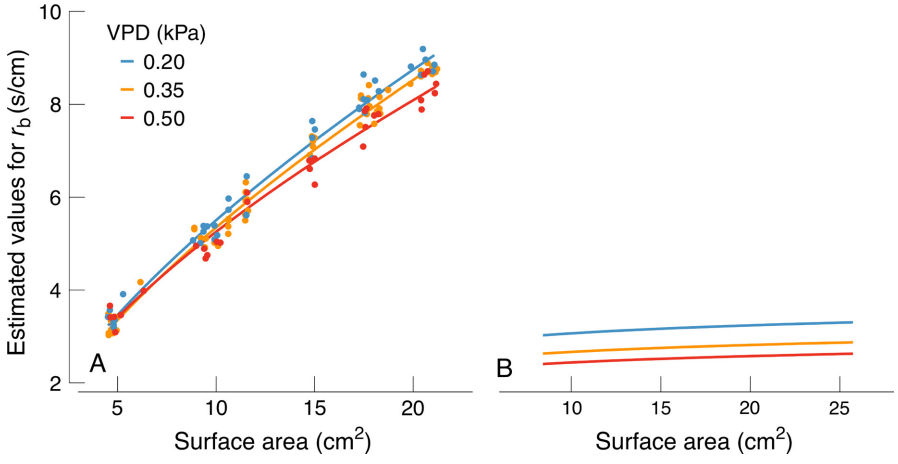

FIG. 3. Estimates of boundary layer resistance varying with vapor pressure deficit (VPD) using (A) empirical and (B) theoretical methods. VPDs are shown in different colors, ranging from blue as the highest VPD to red as the lowest VPD. In both cases, the boundary layer resistance is largest under moist conditions. The two methods differ substantially in the estimates of the boundary layer resistance. [Color figure can be viewed at wileyonlinelibrary.com]

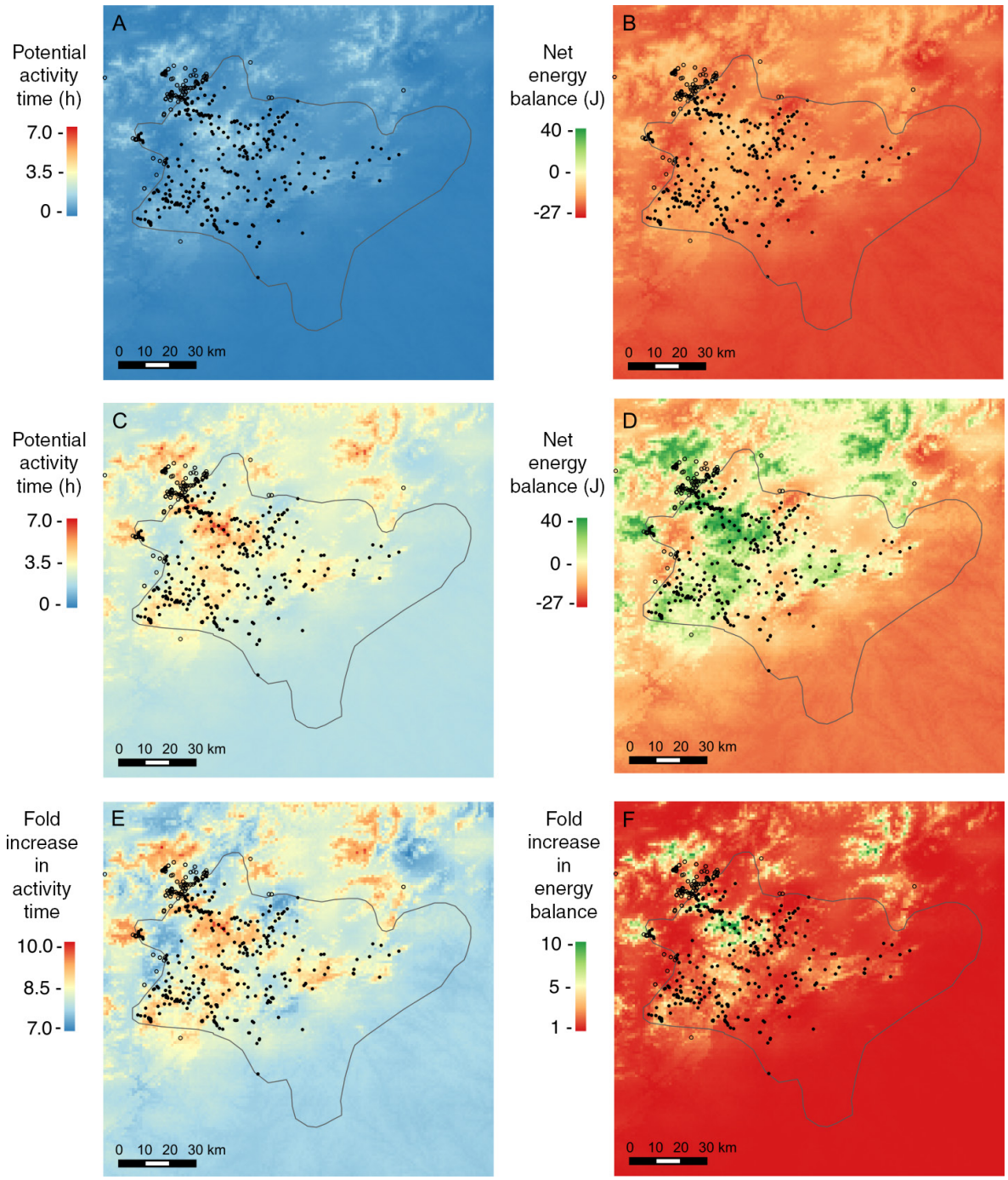

FIG. 4. Estimates of potential activity time and energetics for *Plethodon metcalfi* over a geographical extent (185 × 180 km) at a spatial resolution of 1 km^2 on an average night in August. Without realistic skin and boundary layer resistances, estimates of activity are very low (A) and the majority of estimates of energy balance are negative (B). Incorporating realistic resistances greatly increases estimates of potential activity (C) and many of the high elevation geographic regions are in positive energy balance (D). By using realistic resistances, estimates of activity increased by 7- to 10-fold (E) and energy balance increased by as much as an order of magnitude (F), particularly at the high elevations. The light gray shape represents the distribution of *P. metcalfi*, and the points in panels A and B represent all known captures from 1931 to present day. Solid circles are captures found within the known range of *P. metcalfi*, and open circles refer to captures outside the geographic range that likely represent hybrids, similar species, or true captures. [Color figure can be viewed at wileyonlinelibrary.com]

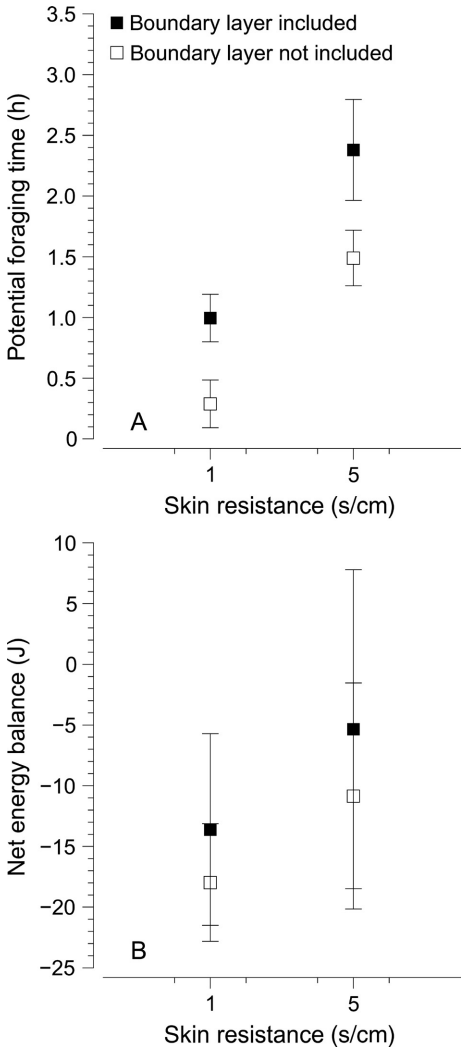

FIG. 5. Estimates of potential activity time and energy balance for an average night in August throughout the entire extent of the geographic area are greatly increased by boundary layer and skin resistance. The figure shows means and standard deviations with and without boundary layer dynamics as well as the influence of no resistance to water loss (r_i = 1 s/cm) and average skin resistance (5 s/cm) calculated from our study using first principles for (A) potential activity time and (B) net energy balance.

compared to cooler months. Our study demonstrates that resistances to water loss can dramatically influence estimates of habitat suitability for salamanders, but the ecological significance of these physical processes are not limited to amphibians.

The importance of the boundary layer depends upon its resistance relative to the skin resistance of an organism. Most birds and amphibians have low skin resistances to water loss (Fig. 7). Therefore, the boundary layer would increase estimates of activity (and thus positive energy balance) by substantially adding to the total resistance to water loss. To date, mechanistic species distribution models do not incorporate boundary layer resistances, despite its potential to influence energetics. Consequently, these models might underestimate suitable habitat because these models would assume higher rates of water loss compared to reality. Some animals, such as reptiles and certain frogs, have adapted high skin resistances to water loss, likely as an evolutionary response to arid habitats (Cox and Cox 2015). With such high skin resistances, the boundary layer of many reptiles would not substantially increase the total resistance to water loss and might be ignored without consequence. However, based on the low skin resistances of many animals, incorporating the boundary layer might improve the performance of physiologically structured species range models.

Our comparison of theoretical and empirical methods demonstrated that first principles improve estimates of skin resistance to water loss. These experiments found that using agar is an ineffective method to determine the boundary layer resistance because it consistently produces negative values of skin resistance. From the perspective of physics, negative resistances are unreasonable because they suggest that salamanders have higher water loss rates than free water. Alternatively, the more plausible explanation is that agar has a resistance. The estimated resistance of agar could be due to hydrophilic interactions of agar (Masuzawa and Sterling 1968) or a change in solute concentrations of the liquid evaporating from the surface of the agar model (Stull 2000). Therefore, the variation of the empirical values of r_b likely reflect these (or other unknown) processes that influence the flux of water vapor. Regardless of the mechanism, our data indicate that agar replicas underestimate the resistance of amphibian skin to water loss. These experiments also suggest calculations for resistance to water loss are more influenced by experimental conditions than previously thought.

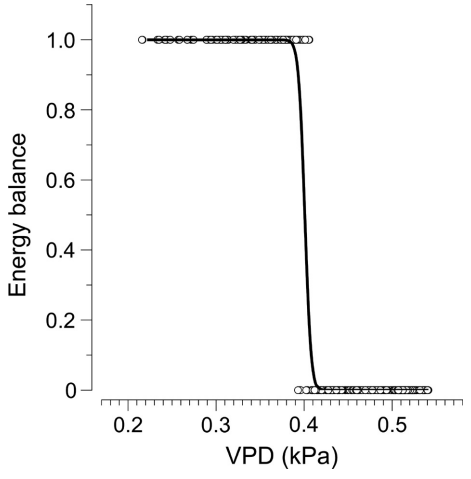

FIG. 6. Vapor pressure deficit (VPD) predicts the energy balance of randomly generated coordinates created within the spatial extent of the species distribution model. In the figure, a low VPD is associated with locations with positive energy balance (a value of 1.0), and high VPD is associated with negative energy balance (a value of 0).

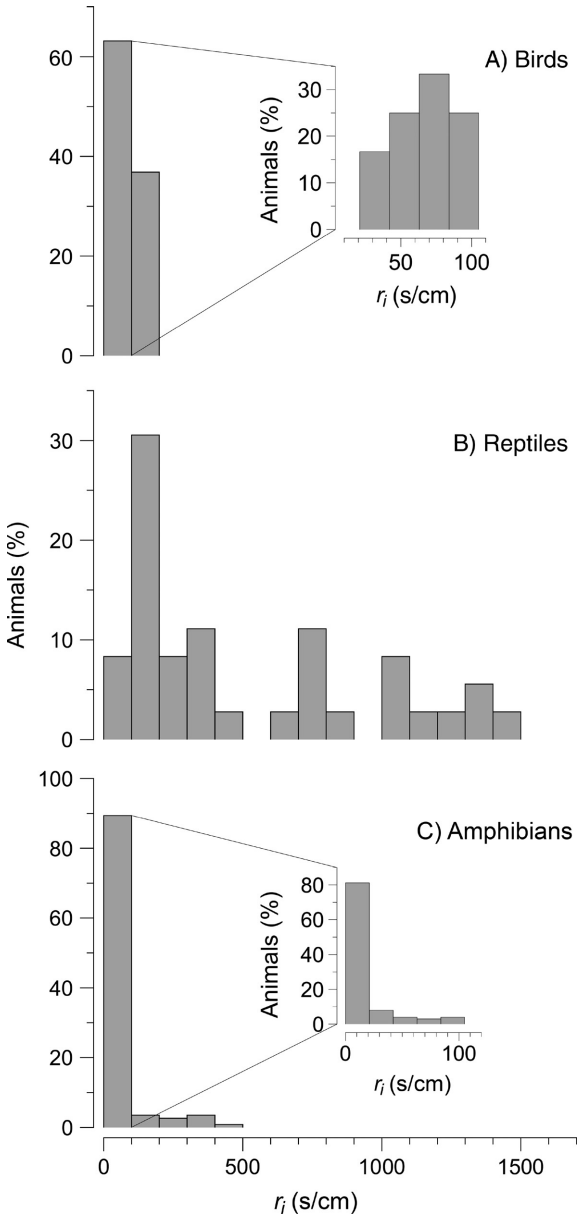

FIG. 7. A frequency distribution plot adapted from Lillywhite (2006) demonstrating that many animals have low skin resistances to water loss. The figure summarizes skin resistances for (A) birds (n = 19), (B) lizards (n = 37), and (C) amphibians (n = 119). The inset figures within the bird and amphibian panels show the distribution of skin resistances below 100 s/cm.

Skin resistance to water loss controls for many environmental factors that influence water loss, but current calculations of r_i ignore important processes that influence rates of water loss. Resistance values are calculated by dividing the water vapor density gradient by the cutaneous water loss rate of the organism (i.e., the flux). For instance, a resistance value of 1.0 would indicate an equivalent gradient and flux. However, the equation to calculate water vapor density gradient is solely a function of the temperature and vapor pressure in the air. In reality, the gradient will be highly influenced by wind speed because it affects the boundary layer where exchange occurs. Simply measuring water loss rates at a higher flow rate (with the same water vapor density gradient) would result in a lower resistance. Similarly, larger body sizes influence the vapor density gradient due to the greater total evaporation water loss at a given flow rate. We attempted to address these problems, but current calculations are parameterized for evaporation from crops, soil, or pure water on hydrophobic surfaces and appear to be inappropriate for properly correcting water vapor density gradients (Birdi et al. 1989, Monteith and Unsworth 2013). Future research is required to resolve the contribution of wind speed to the gradient driving evaporative water loss. Because flow rate and body size can confound analyses, comparative studies of skin resistance to water loss must incorporate flow rates and body sizes as covariates. These dynamics also suggest the use of physical surrogates in nature should also be interpreted cautiously.

Physical replicas of animals can be a valuable tool to characterize the environmental conditions experienced by an organism (Bartholomew and Tucker 1963, Lee and Badham 1963, Bakken 1976). These replicas are tools used to understand how animals respond to their thermal environment (Heath 1964), but high water loss rates complicate the use of replicas in amphibians. To date, replicas have been implemented using agar (Roznik and Alford 2014), saturated plaster models (Peterman et al. 2013), gravity-fed plaster models (Tracy et al. 2007), copper models surrounded by wet cloth (Bartelt and Peterson 2005), and synthetic foam (Hasegawa et al. 2005). Each surrogate has its disadvantages, but more importantly, some surrogates far outperform others (Tracy et al. 2007). Agar, saturated plaster, and synthetic foam have a limited lifetime in the field as desiccation increases variation of water loss rates (Peterman et al. 2013), which reduces the accuracy of mimicking water loss physiology over time. Each replica also requires specific concentrations or water content necessary to mimic their study organism (Hasegawa et al. 2005). Measuring water loss gravimetrically can also be hindered by the low resolution of some scales (Bartelt and Peterson 2005), which would prevent measurements on small organisms. From a physiological perspective, physical surrogates might only be helpful to qualitatively understanding skin resistance to water loss (Roznik and Alford 2014). Instead of surrogates, we recommend ecologists use the available calculations in the literature to characterize humid operative temperatures (Tracy 1975, 1976, 1982, Caruso et al. 2014). These equations can be used to understand ecology by linking environmental characteristics to energetics of their study organism. Of course, these estimates can then be compared to ecological studies in the field to validate their effectiveness.

Historically, water loss physiology has been characterized as one-dimensional. The majority of studies have

concluded that amphibians have a negligible resistance to water loss (Spight 1967, Spotila 1972, Spotila and Berman 1976). Unfortunately, these conclusions were based upon a flawed material used to estimate skin resistance. We provide methods that might uncover variation of skin resistance to water loss in salamander populations. Moreover, to effectively measure r_i, water loss studies need to adjust relative humidities to avoid confounding temperature treatments with different VPDs. By adopting these methods, recent research found novel physiological responses of water loss to warm temperature (Riddell and Sears 2015). The proposed methods might also explain identify physiological mechanisms underlying patterns of body size, population declines, and species distributions (Rovito et al. 2009, Caruso and Lips 2012, Gifford and Kozak 2012, Caruso et al. 2014). More importantly, water loss has a pervasive influence on the ecology of organisms throughout their life cycle (Bartholomew and Tucker 1963). Therefore, our approach has the potential to identify the physical and biological mechanisms involved in shaping species geographic distributions for an array of taxa.

Acknowledgments

I would like to thank Clemson's Biology Writing Group for their comments on this paper. I would also like to thank Stanlee Miller for providing museum specimens to cast the agar replicas of our salamanders. I would also like to thank the Highlands Biological Station and their Grant-in-Aid program for supporting these experiments. Salamanders were collected with the required licenses from the North Carolina Wildlife Commission (13-SC00746). Experiments were conducted with approval from the Institute of Animal Care and Use Committee (2013-022). The authors do not have any conflicts of interest with the presented material. I am also very grateful for the comments provided by the anonymous reviewers that greatly improved the manuscript.

Literature Cited

Amey, A. P., and G. C. Grigg. 1995. Lipid-reduced evaporative water loss in two arboreal hylid frogs. Comparative Biochemistry and Physiology Part A: Physiology 111:283–291.

Anderson, D. B. 1936. Relative humidity or vapor pressure deficit. Ecology 17:277–282.

Bakken, G. S. 1976. A heat transfer analysis of animals: unifying concepts and the application of metabolism chamber data to field ecology. Journal of Theoretical Biology 60: 337–384.

Bartelt, P. E., and C. R. Peterson. 2005. Physically modeling operative temperatures and evaporation rates in amphibians. Journal of Thermal Biology 30:93–102.

Bartholomew, G. A., and V. A. Tucker. 1963. Control of changes in body temperature, metabolism, and circulation by the agamid lizard, *Amphibolurus barbatus*. Physiological Zoology 36:199–218.

Bell, G. P. 1990. Birds and mammals on an insect diet: a primer on diet composition analysis in relation to ecological energetics. Studies in Avian Biology 13:416–422.

Bellis, E. D. 1962. The influence of humidity on wood frog activity. American Midland Naturalist 68:139.

Bernstein, M. H., D. M. Hudson, J. M. Stearns, and R. W. Hoyt. 1977. Measurement of evaporative water loss in small animals by dew-point hygrometry. Journal of Applied Physiology 43:382–385.

Birdi, K. S., D. T. Vu, and A. Winter. 1989. A study of the evaporation rates of small water drops placed on a solid surface. Journal of Physical Chemistry 93:3702–3703.

Buckley, L. B., M. C. Urban, M. J. Angilletta, L. G. Crozier, L. J. Rissler, and M. W. Sears. 2010. Can mechanism inform species' distribution models? Ecology Letters 13:1041–1054.

Buttemer, W. 1990. Effect of temperature on evaporative water loss of the Australian tree frogs *Litoria caerulea* and *Litoria chloris*. Physiological Zoology 63:1043–1057.

Caruso, N. M., and K. R. Lips. 2012. Truly enigmatic declines in terrestrial salamander populations in Great Smoky Mountains National Park. Diversity and Distributions 19:38–48.

Caruso, N. M., M. W. Sears, D. C. Adams, and K. R. Lips. 2014. Widespread rapid reductions in body size of adult salamanders in response to climate change. Global Change Biology 20:1751–1759.

Christian, K., and D. Parry. 1997. Reduced rates of water loss and chemical properties of skin secretions of the frogs *Litoria caerulea* and *Cyclorana australis*. Australian Journal of Zoology 45:13–20.

Cox, C. L., and R. M. Cox. 2015. Evolutionary shifts in habitat aridity predict evaporative water loss across squamate reptiles. Evolution 69:2507–2516.

Crozier, L., and G. Dwyer. 2006. Combining population-dynamic and ecophysiological models to predict climate-induced insect range shifts. American Naturalist 167:853–866.

de V Weir, J. B. 1949. New methods for calculating metabolic rate with special reference to protein metabolism. Journal of Physiology 109:1–9.

Feder, M. E., and W. W. Burggren. 1992. Environmental physiology of the amphibians. The University of Chicago Press, Chicago, Illinois, USA.

Feder, M. E., and P. L. Londos. 1984. Hydric constraints upon foraging in a terrestrial salamander, *Desmognathus ochrophaeus* (Amphibia: Plethodontidae). Oecologia 64: 413–418.

Fox, J., and S. Weisberg. 2011. An R companion to applied regression. Sage, Thousand Oaks, California, USA. http://socserv.socsci.mcmaster.ca/jfox/Books/Companion

Gates, D. M. 1980. Biophysical ecology. Dover Publications, Mineola, New York, USA.

Gifford, M. E., and K. H. Kozak. 2012. Islands in the sky or squeezed at the top? Ecological causes of elevational range limits in montane salamanders. Ecography 35:193–203.

Grinnell, J. 1917. The niche-relationships of the California thrasher. Auk 34:427–433.

Hasegawa, M., Y. Suzuki, and S. Wada. 2005. Design and performance of a wet sponge model for amphibian thermal biology. Current Herpetology 24:27–32.

Heath, J. E. 1964. Reptilian thermoregulation: evaluation of field studies. Science 146:784–785.

Highton, R., and R. B. Peabody. 2000. Geographic protein variation and speciation in salamanders of the *Plethodon jordani* and *Plethodon glutinosus* complexes in the southern Appalachian Mountains with the description of four new species. Pages 31–93 *in* R. C. Bruce, R. G. Jaegar, and L. D. Houck, editor. The biology of plethodontid salamanders. Springer US, Boston, Massachusetts, USA.

Hillman, S. S., P. Withers, R. Drewes, and S. Hillyard. 2009. Ecological and environmental physiology of amphibians. Oxford University Press, New York, New York, USA.

Kearney, M. R., A. P. Isaac, and W. P. Porter. 2014. microclim: global estimates of hourly microclimate based on long-term monthly climate averages. Scientific Data 1:140006.

Kearney, M. R., and W. P. Porter. 2004. Mapping the fundamental niche: physiology, climate, and the distribution of a nocturnal lizard. Ecology 85:3119–3131.

Kearney, M. R., and W. Porter. 2009. Mechanistic niche modelling: combining physiological and spatial data to predict species' ranges. Ecology Letters 12:334–350.

Langsrud, Ø. 2003. ANOVA for unbalanced data: use Type II instead of Type III sums of squares. Statistics and Computing 13:163–167.

Lee, A. K., and J. A. Badham. 1963. Body temperature, activity, and behavior of the agamid lizard, *Amphibolurus barbatus*. Copeia 1963:387–394.

Lillywhite, H. B. 2006. Water relations of tetrapod integument. Journal of Experimental Biology 209:202–226.

Masuzawa, M., and C. Sterling. 1968. Gel–water relationships in hydrophilic polymers: thermodynamics of sorption of water vapor. Journal of Applied Polymer Science 12: 2023–2032.

Merchant, H. C. 1970. Estimated energy budget of the red-backed salamander, *Plethodon cinereus*. University Microfilms International, Ann Arbor, Michigan, USA.

Monteith, J. L., and M. H. Unsworth. 2013. Principles of environmental physics: plants, animals, and the atmosphere. Fourth edition. Academic Press, Kidlington, UK.

Olejnik, S., and J. Algina. 2003. Generalized eta and omega squared statistics: measures of effect size for some common research designs. Psychological Methods 8:434–447.

Peterman, W. E., J. L. Locke, and R. D. Semlitsch. 2013. Spatial and temporal patterns of water loss in heterogeneous landscapes: using plaster models as amphibian analogues. Canadian Journal of Zoology 91:135–140.

Python Software Foundation. 2015. Python version 2.7. Available from URL: http://www.python.org (Accessed 4/26/2015).

Quantum GIS Development Team. 2015. Quantum GIS Geographic Information System. Open Source Geospatial Foundation Project. http://qgis.osgeo.org

R Core Team. 2015. R: a language and environment for statistical computing. R Foundation for Statistical Computing, Vienna, Austria. www.r-project.org

Riddell, E. A., and M. W. Sears. 2015. Geographic variation of resistance to water loss within two species of lungless salamanders: implications for activity. Ecosphere 6: Article 86.

Rovito, S. M., G. Parra-Olea, C. R. Vásquez-Almazán, T. J. Papenfuss, and D. B. Wake. 2009. Dramatic declines in neotropical salamander populations are an important part of the global amphibian crisis. Proceedings of the National Academy of Sciences USA 106:3231–3236.

Roznik, E. A., and R. A. Alford. 2014. Using pairs of physiological models to estimate temporal variation in amphibian body temperature. Journal of Thermal Biology 45:22–29.

Scheiner, S. M. 2010. Towards a conceptual framework for biology. Quarterly Review of Biology 85:293–318.

Seebacher, F., and R. A. Alford. 2002. Shelter microhabitats determine body temperature and dehydration rates of a terrestrial amphibian (*Bufo marinus*). Journal of Herpetology 36:69–75.

Spight, T. M. 1967. The water economy of salamanders: water uptake after dehydration. Comparative Biochemistry and Physiology 20:767–771.

Spotila, J. R. 1972. Role of temperature and water in the ecology of lungless salamanders. Ecological Monographs 42:95–125.

Spotila, J. R., and E. N. Berman. 1976. Determination of skin resistance and the role of the skin in controlling water loss in amphibians and reptiles. Comparative Biochemistry and Physiology Part A: Physiology 55:407–411.

Stull, R. 2000. Meteorology for scientists and engineers. Second edition. Brooks/Cole, Pacific Grove, California, USA.

Tracy, C. R. 1975. Water and energy relations of terrestrial amphibians: insights from mechanistic modeling. Pages 325–346 *in* D. M. Gates and R. B. Schmerl, editor. Perspectives of biophysical ecology. Springer Berlin Heidelberg, Berlin, Heidelberg, Germany.

Tracy, C. R. 1976. A model of the dynamic exchanges of water and energy between a terrestrial amphibian and its environment. Ecological Monographs 46:293–326.

Tracy, C. R. 1982. Biophysical modeling in reptilian physiology and ecology. Pages 275–321 *in* C. Gans and F. H. Pough, editors. Biology of the Reptilia. Academic Press, London, UK.

Tracy, C. R., G. Betts, C. R. Tracy, and K. A. Christian. 2007. Plaster models to measure operative temperature and evaporative water loss of amphibians. Journal of Herpetology 41: 597–603.

Tracy, C. R., K. A. Christian, and C. R. Tracy. 2010*a*. Not just small, wet, and cold: effects of body size and skin resistance on thermoregulation and arboreality of frogs. Ecology 91: 1477–1484.

Tracy, C. R., W. R. Welch, B. Pinshow, and W. P. Porter. 2010*b*. Properties of air: a manual for use in biophysical ecology. Fourth edition. University of Wisconsin-Madison, Technical Report No. 1.

Whitford, W. G., and V. H. Hutchison. 1967. Body size and metabolic rate in salamanders. Physiological Zoology 40: 127–133.

Wygoda, M. L. 1984. Low cutaneous evaporative water loss in arboreal frogs. Physiological Zoology 57:329–337.

Young, J. E., K. A. Christian, S. Donnellan, C. R. Tracy, and D. Parry. 2005. Comparative analysis of cutaneous evaporative water loss in frogs demonstrates correlation with ecological habits. Physiological and Biochemical Zoology 78:847–856.

Young, J. E., C. R. Tracy, K. A. Christian, and L. J. McArthur. 2006. Rates of cutaneous evaporative water loss of native Fijian frogs. Copeia 2006:83–88.

Supporting Information

Additional supporting information may be found in the online version of this article at http://onlinelibrary.wiley.com/doi/10.1002/ecm.1240/full

Data Availability

Data available from the Dryad Digital Repository: https://doi.org/10.5061/dryad.481g3